Eletrônica de Potência
Open Journal of Power Electronics

Received July 31, 2024; accepted December 12, 2024; Date of publication January 17, 2025.
The review of this paper was arranged by Associate Editor Mokhtar A. Ahmed and Editor-in-Chief Heverton A. Pereira.
Digital Object Identifier http://doi.org/10.18618/REP.e202507

Comparison Between Hysteresis and Predictive Control with Optimized Vector Selection for Direct Power Control to a Shunt Active Power Filter

Ruben da C. Ferreira[1], Pedro H. de M. Martins[2], Nady Rocha[1], Edison R. C. da Silva[1], Victor F. M. B. Melo[2]

[1]Federal University of Paraíba, Department of Electrical Engineering, João Pessoa – PB, Brazil.
[2]Federal University of Paraíba, Department of Renewable Energies Engineering, João Pessoa – PB, Brazil.

e-mail: ruben.ferreira@cear.ufpb.br; pedro.martins@cear.ufpb.br; nadyrocha@cear.ufpb.br; ercdasilva@gmail.com; victor@cear.ufpb.br

ABSTRACT In this paper, the performance of a shunt active power filter using direct power control based on the hysteresis method and model predictive control is discussed. Furthermore, an optimized vector selection is presented for model predictive control. This paper's objective is to evaluate the processing time, reduction of harmonic components that would be injected into the electrical grid by a non-linear load, power semiconductor losses, average switching frequency and root mean square error for the control variables. The comparison uses the same system model and parameters for both strategies. Simulation and experimental results are presented. Using the strategy discussed in this paper, it was possible to reduce harmonic components in the electrical grid, with reduced time for vector selection.

KEYWORDS Active power filter, harmonic components, predictive control, hysteresis control, power quality.

I. INTRODUCTION

Problems related to power quality have gained attention in recent years, especially when it comes to the use of non-linear and/or unbalanced loads, leading to the presence of harmonic components in the currents and voltages of the electrical grid [1]. In industry, some examples of non-linear loads are uninterruptible power supplies, variable frequency drives and diode bridge rectifiers, see [2] for more examples. Harmonics cause various issues, including overheating of electrical equipment, blown capacitor fuses, distorted voltage waveforms, low power factor, eddy current losses in transformers, oscillating torque in electrical machines, and decreased system efficiency [3]. Shunt Active Power Filters (SAPF) can mitigate these harmonics and are easily integrated into existing industrial power systems, making them a widely used solution [4].

Reducing current ripple in active power filters is essential to ensure the efficiency, reliability, and safety of electrical and electronic systems, in addition to improving the quality of the energy supplied and protecting system components. Therefore, when it comes to active filters, one of the elements that is essential for reducing current ripple is the inductor. In [5], the calculation is presented for inductance for the use of a control strategy with Pulse Width Modulation (PWM). However, the relation obtained in [5] cannot be applied for the Predictive Power Control (PPC) because this control method does not have fixed switching frequency. In this way, the present paper will show the solution for this case.

One of the techniques used to compensate for harmonics using an SAPF is Direct Power Control (DPC). DPC, when compared with PWM [6], shows superior performance in terms of dynamic response and the absence of current control loops in the control structure. Predictive Power Control (PPC), uses the Finite Control Set - Model Predictive Control (FCS-MPC) strategy with power being the control variable, where the optimal voltage vector is determined by a control scheme that minimizes a cost function. According to [7], control systems using FCS-MPC allow ease of implementation, fast dynamic response and flexibility in defining the control objective.

On the other hand, according to [8], FCS-MPC exhibits high computational cost, posing a significant challenge for its implementation in power electronics applications. Despite technological advancements in processors processing power over the years, high computational cost remains a critical challenge for FCS-MPC utilization, as evidenced by studies presented in [9]. Thus, in [10], a Four-Wire Shunt Active Power Filter (FW-SAPF) is presented with a significant reduction in the number of tests required in FCS-MPC by implementing a novel vector optimization strategy. In [11], a parallel single-phase to three-phase drive system with two single-phase rectifiers using Modulated Model Predictive Control with reduction of tests based on the vector plan is presented.

In this context, this article presents DPC and PPC strategies for a SAPF using a three-phase inverter. This article is

an expanded version of [12], which presents a method to reduce processing time for identifying the optimal vector. The comparison between the strategies is carried out for a system containing a SAPF connected to the electrical grid with the presence of a non-linear load. The reduction of harmonic components that would be injected into the electrical grid by a non-linear load, power semiconductor losses, average switching frequency and root mean square error for the control variables are evaluated. To validate the strategies, simulation and experimental results are presented. In summary, the main improvements of this paper compared with [12] are as follows:

I) Proposing a new strategy using the PPC based on the SAPF reference voltage;
II) Reduction in processing time of approximately 20% when compared with the strategy presented in [12];
III) Calculation of the reference voltage based on the reference active and reactive power;
IV) Comparison between the strategies presented in [12] with the one proposed in this article;
V) Total Harmonic Distortion (THD);
VI) Addition of simulation and experimental results for load transient.

This paper is organized as follows. In Section II, the System Model is presented, detailing the mathematical formulations for the system in continuous and discrete time. Section III discusses the control strategy for Direct Power Control and Section IV for Predictive Power Control with optimized vector selection. Section V focuses on simulation results, where the control strategies are validated. In section VI, a comparison between DPC and PPC is performed with results obtained by simulation. Section VII focuses on experimental results for practical validation. Finally, Section VIII presents the Conclusion, summarizing the main contributions of the work.

II. SYSTEM MODEL

The shunt active power filter configuration is shown in Fig. 1. Connected to the grid, there is a non-linear load. In this way, the SAPF is responsible for minimizing the harmonics injected into the electrical grid. According to Fig. 1, the SAPF system equations are:

$$e_{gu} = -r_f i_{fu} - l_f \frac{di_{fu}}{dt} + v_{fu} \tag{1}$$

$$v_{fu} = v_{u0} + v_{0g} \tag{2}$$

where $u = \{1, 2, 3\}$, e_{gu} is the voltage in the electrical grid, r_f and l_f are, respectively, the resistance and inductance of the RL-filter, v_{fu} is the voltage of SAPF, v_{u0} is the inverter pole voltage, v_{0g} is the homopolar voltage. The instantaneous active (P_g) and reactive (Q_g) power of the grid are:

$$P_g = P_l - P_f \tag{3}$$

$$Q_g = Q_l - Q_f \tag{4}$$

where P_l and Q_l are the instantaneous active and reactive power of the non-linear load and P_f and Q_f are the instantaneous active and reactive power of the SAPF.

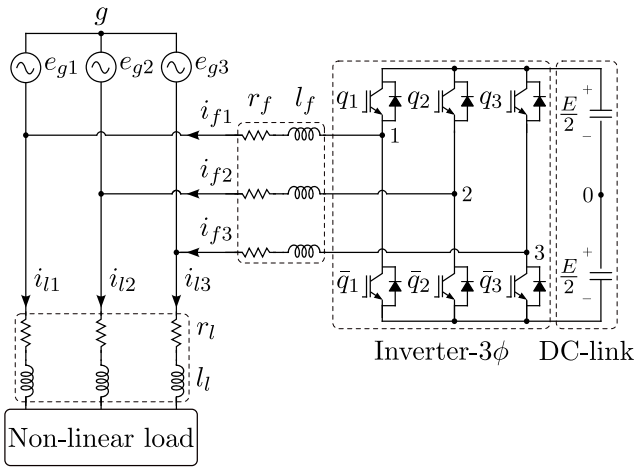

FIGURE 1. Shunt active power filter.

The grid voltage equation presented in (1) can be referred to the $\alpha\beta$ axes in a stationary reference frame to facilitate the strategy control. Applying the change to the stationary reference $\alpha\beta$, it is verified that:

$$e_{g\alpha} = -r_f i_{f\alpha} - l_f \frac{di_{f\alpha}}{dt} + v_{f\alpha} \tag{5}$$

$$e_{g\beta} = -r_f i_{f\beta} - l_f \frac{di_{f\beta}}{dt} + v_{f\beta} \tag{6}$$

The voltages $v_{f\alpha}$ and $v_{f\beta}$ are dependent on the inverter switching state and the DC-link voltage E, i.e.:

$$v_{f\alpha} = E\sqrt{\frac{2}{3}}\left(q_1 - \frac{q_2}{2} - \frac{q_3}{2}\right) \tag{7}$$

$$v_{f\beta} = \frac{E}{\sqrt{2}}(q_2 - q_3) \tag{8}$$

where q_u represents the switching states of the inverter. According to Table 1, the SAPF $\alpha\beta$ voltage components have five and three levels, respectively.

TABLE 1. Switching states for SAPF voltages in the stationary frame

$\vec{v}$	q_1	q_2	q_3	$v_{f\alpha}$	$v_{f\beta}$
V_0	0	0	0	0	0
V_1	0	0	1	$-E/\sqrt{6}$	$-E/\sqrt{2}$
V_2	0	1	0	$-E/\sqrt{6}$	$E/\sqrt{2}$
V_3	0	1	1	$-E\sqrt{2/3}$	0
V_4	1	0	0	$E\sqrt{2/3}$	0
V_5	1	0	1	$E/\sqrt{6}$	$-E/\sqrt{2}$
V_6	1	1	0	$E/\sqrt{6}$	$E/\sqrt{2}$
V_7	1	1	1	0	0

A. DISCRETE MODEL

The SAPF instantaneous active and reactive power can be obtained through the components of the voltage and current in the stationary reference frame, that is:

$$P_f = e_{g\alpha} i_{f\alpha} + e_{g\beta} i_{f\beta} \tag{9}$$

$$Q_f = e_{g\beta} i_{f\alpha} - e_{g\alpha} i_{f\beta} \tag{10}$$

Deriving (9) and (10) and substituting the differential terms of (5) and (6) there is:

$$\frac{dP_f}{dt} = -\frac{r_f}{l_f} P_f - \omega_g Q_f + \frac{e_{g\alpha} v_{f\alpha} + e_{g\beta} v_{f\beta} - V_M^2}{l_f} \tag{11}$$

$$\frac{dQ_f}{dt} = \omega_g P_f - \frac{r_f}{l_f} Q_f + \frac{e_{g\beta} v_{f\alpha} - e_{g\alpha} v_{f\beta}}{l_f} \tag{12}$$

where ω_g is the angular frequency of the grid and $V_M^2 = e_{g\alpha}^2 + e_{g\beta}^2$. In [13], different discretization methods are presented for use in predictive control. Among the analyzed methods, Euler was selected for use in this paper due to its easy implementation and good response. Therefore, using the forward Euler method in (11) and (12), the discrete model of SAPF for the second horizon and sampling time T_s is:

$$P_f[k_2] = -\omega_g T_s Q_f[k_1] + P_f[k_1]\left(1 - \frac{r_f}{l_f} T_s\right) + \frac{e_{g\alpha}[k_1] v_{f\alpha}[k_1] + e_{g\beta}[k_1] v_{f\beta}[k_1] - V_M^2}{l_f} T_s \tag{13}$$

$$Q_f[k_2] = \omega_g T_s P_f[k_1] + Q_f[k_1]\left(1 - \frac{r_f}{l_f} T_s\right) + \frac{e_{g\beta}[k_1] v_{f\alpha}[k_1] - e_{g\alpha}[k_1] v_{f\beta}[k_1]}{l_f} T_s \tag{14}$$

where $k_1 = k + 1$ and $k_2 = k + 2$, indicating the first and second horizons. The second horizon is necessary to compensate for computational delays, and by using this method the current ripple is considerably reduced without affecting the dynamics of the control.

Thus, the discrete model for instantaneous power of the electrical grid is obtained as:

$$P_g[k_2] = P_l[k_2] - P_f[k_2] \tag{15}$$

$$Q_g[k_2] = Q_l[k_2] - Q_f[k_2] \tag{16}$$

The instantaneous active and reactive power of the non-linear load in the second horizon, due to the use of a small sampling period T_s, can be obtained by approximation to the values at the discrete instant k, that is, $P_l[k] \approx P_l[k+2]$ and $Q_l[k] \approx Q_l[k+2]$. Another option is to use the Lagrange Extrapolation presented in [14]. The same can be used for grid voltages.

B. FILTER INDUCTOR DESIGN

According to [5], the resistance has no impact on the current ripple, then to obtain the inductance calculation it is possible to neglect the resistance in (1), then the reference of the grid voltage can be considered as:

$$e_{gu}^* = -l_f \frac{di_{fu}^*}{dt} + v_{fu}^* \tag{17}$$

Consider that the current and voltage in the SAPF are equal to a reference value with the presence of a ripple, i.e.:

$$i_{fu} = i_{fu}^* + \Delta i_{fu} \tag{18}$$

$$v_{fu} = v_{fu}^* + \Delta v_{fu} \tag{19}$$

Thus, using (18) and (19) and making the difference between (17) and (1) (without r_f) and as the grid voltage is fixed, that is, $e_{gu} = e_{gu}^*$, then:

$$l_f \frac{\Delta v_{fu}}{dt} = \Delta i_{fu} \tag{20}$$

Solving (20) for l_f, the inductance used in the RL filter can be calculated as:

$$l_f = \frac{1}{\Delta i_{fu}} \int_{t_0}^{t_0+T_s} \Delta v_{fu}\, dt \tag{21}$$

where t_0 is any instant of time and T_s is the sampling period. In the FCS-MPC, the SAPF voltage changes once every T_s, and as $\Delta v_{fu} = E/3$ (for changing a voltage level) for three-phase inverter, then it is found that:

$$l_f = \frac{E}{3 f_s \Delta I_f} \tag{22}$$

where $\Delta I_f = \Delta I_{fu}$ is the ripple to the current of SAPF and f_s is the sampling frequency. From [15] and [16], ΔI_f is calculated considering the following:

1) The SAPF power (P_{SAPF}) is equal to 125% of the load;
2) The current ripple is equal to 10% of the SAPF current;
3) SAPF current is $I_f = P_{\text{SAPF}}(\text{VA})/E$.

III. DIRECT POWER CONTROL

For benchmarking purposes, this paper uses the Direct Power Control (DPC) proposed by [17]. This type of control uses active and reactive power as control variables. The instantaneous active power reference (P_f^*) is generated from the existing instantaneous load active power and the power processed by the shunt active power filter obtained by DC-link control. As shown in Fig. 2, the starting point is to calculate the load's instantaneous active power (P_l). This is followed by the instantaneous active power ripple obtained from the difference between the instantaneous active power and the average active power (signal resulting from the low-pass filter). Finally, the injected reference active power is obtained from the difference between the load's alternating instantaneous active power and the power resulting from the DC-link control.

The instantaneous reactive power reference (Q_f^*) is also generated by the instantaneous reactive power resulting from the non-linear load. The reference for reactive power corresponds directly to the instantaneous reactive power Q_l as illustrated in Fig. 2. Furthermore, there is no contribution of reactive power from the DC-link.

In this way, the integration between the power control repetition loop and the switching function for the DPC was developed, as shown in Fig. 2. For DPC, two hysteresis comparators, one for active power and the other for reactive power, associated with the Phase-Locked Loop (PLL), send

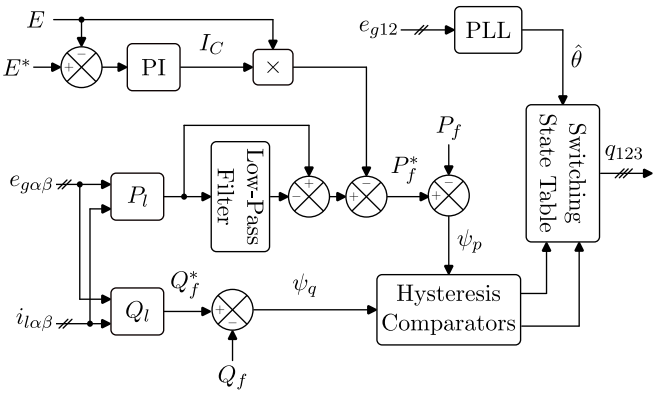

FIGURE 2. DPC control diagram.

gating signals the inverter transistors (q_1, q_2, q_3, $\bar{q}_1$, $\bar{q}_2$ and $\bar{q}_3$). The differences between the instantaneous powers injected by the active power filter and the instantaneous powers of the non-linear load (ψ_p and ψ_q) are limited within a hysteresis band. The PLL model proposed by [18] provides information about the phase $\hat{\theta}$ of the power grid.

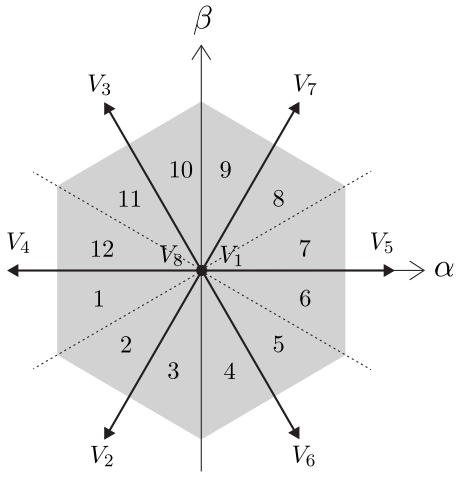

FIGURE 3. Method of division into twelve sectors in the $\alpha\beta$ plane.

The $\alpha\beta$ plane is divided into twelve equidistant sectors as illustrated in Fig. 3. The appropriate voltage vector selection was the vector that, after its application, leads ψ_p and ψ_q to towards zero. When $\psi_p < 0$ and $\psi_q < 0$, it was necessary to apply a voltage vector that would cause the inverter to act with an inductive effect and as a load (consuming power). So the possible application was the vector V_2 (001). When $\psi_p < 0$ and $\psi_q \geq 0$, it was necessary to apply a voltage vector that would make the inverter act with a capacitive effect and as a load (consuming power). Thus, the application possibilities were the vectors V_5 (100) and V_6 (101). When $\psi_p \geq 0$ and $\psi_q < 0$, it was necessary to apply a voltage vector that would make the inverter act with an inductive effect and as a power source. Thus, the application possibilities were the vectors V_3 (010) and V_4 (011). When $\psi_p \geq 0$ and $\psi_q \geq 0$, it was necessary to apply a voltage vector that would make the inverter act with a capacitive effect and as a power source. The possible application was therefore the vector V_7 (110). Table 2 shows the switching functions determined by instantaneous power comparison for a sinusoidal electrical grid.

TABLE 2. Switchings determined by instantaneous power comparison

	S_1	S_2	S_3	S_4	S_5	S_6
$\psi_p < 0$ $\psi_q < 0$	001	001	101	101	100	100
$\psi_p < 0$ $\psi_q \geq 0$	100	100	110	110	010	010
$\psi_p \geq 0$ $\psi_q < 0$	010	011	011	001	001	101
$\psi_p \geq 0$ $\psi_q \geq 0$	110	010	010	011	011	001
	S_7	S_8	S_9	S_{10}	S_{11}	S_{12}
$\psi_p < 0$ $\psi_q < 0$	110	110	010	010	011	011
$\psi_p < 0$ $\psi_q \geq 0$	011	011	001	001	101	101
$\psi_p \geq 0$ $\psi_q < 0$	101	100	100	110	110	010
$\psi_p \geq 0$ $\psi_q \geq 0$	001	101	101	100	100	110

IV. PREDICTIVE POWER CONTROL

Fig. 4 shows the control diagram for the predictive power control. The processes described in the diagram are used for DC-link control, decrease of harmonic distortion and correction of the power factor in the electrical grid.

According to [19], when a PI controller regulates the DC-link, the predictive control has a loss in the dynamic response, due to the PI controller having a lower speed response than the predictive control. Because of that, the control strategy does not use a PI controller to regulate the DC-link. To obtain the active power reference, the relations presented in [19] are used:

$$P_g^*[k_2] = P_l^*[k_2] - \hat{P}_{DC} \tag{23}$$

$$\hat{P}_{DC} = \frac{C}{2NT_s}\left(E^2[k_1] - E^{*2}\right) \tag{24}$$

where $P_l^*[k_2]$ is the reference active power of the load in the second horizon, obtained using a digital low-pass filter with a cut-off frequency equal to the fundamental of the grid, $\hat{P}_{DC}$ is the required change in the active power flow to regulate the voltage at the desired value, C is the equivalent capacitance in DC-link, E^* is the reference voltage of the DC-link and, according to [19], N denotes the number of time steps required for reaching the target.

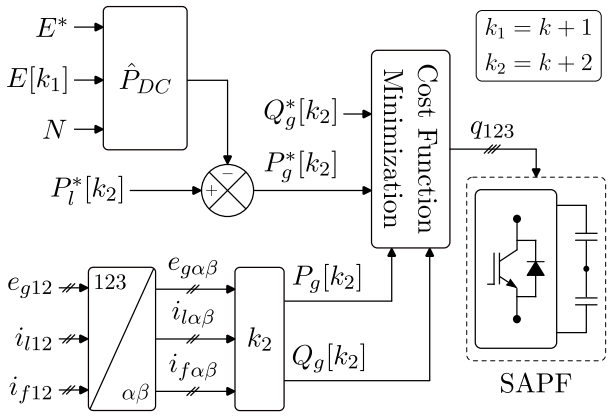

FIGURE 4. PPC control diagram.

The reference reactive power in the electrical grid is equal to 0, to ensure a unity power factor of the system. Thus, for each selected switching state, the discrete active and reactive powers are compared with their respective reference powers. The best vector is the one that minimizes:

$$g_j = \left|P_g^*[k_2] - P_g^j[k_2]\right| + \left|Q_g^*[k_2] - Q_g^j[k_2]\right| \qquad (25)$$

where g_j is the cost function and $j = \{1, 2, \cdots, 8\}$ indicate the vector test.

Fig. 5 shows flowchart for the PPC with optimized vector selection applied to the SAPF. The general control procedure can be described as:

1) Grid voltage measurements (e_{g1} and e_{g2}), SAPF currents (i_{f1} and i_{f2}), load currents (i_{l1} and i_{l2}) and DC-link voltage (E);
2) Change to the stationary reference frame $\alpha\beta$ and advance one step into the first horizon;
3) Predicting $P_g[k_1]$, $Q_g[k_1]$, $P_l[k_2]$ and $Q_l[k_2]$;
4) Calculation of $P_l^*[k_2]$ and $\hat{P}_{DC}$ to be used in (23);
5) Calculation of the reference active power in the electrical grid for the second horizon;
6) Calculation of v_{f1}^*, v_{f2}^* and v_{f3}^*;
7) Preselected voltage vectors;
8) Initial value for $g_{\min}$;
9) Structure in the for:
   a) Calculation of the components α and β of $v_{f\alpha\beta}$, for the second horizon, using (7) and (8), based on Table 1 for each iteration;
   b) Calculation of active and reactive power in the electrical grid using (13) and (14);
   c) Cost function calculation with (25);
   d) Checking and storing the smallest value of the cost function and the vector j at which minimizes (25).
10) Applying the switching state obtained by PPC.

A. OPTIMIZED VECTOR SELECTION

According to [20], it is possible to reduce the amount of vectors tested in a three-phase rectifier based on the reference voltages of the legs. Thus, obtaining the reference voltages

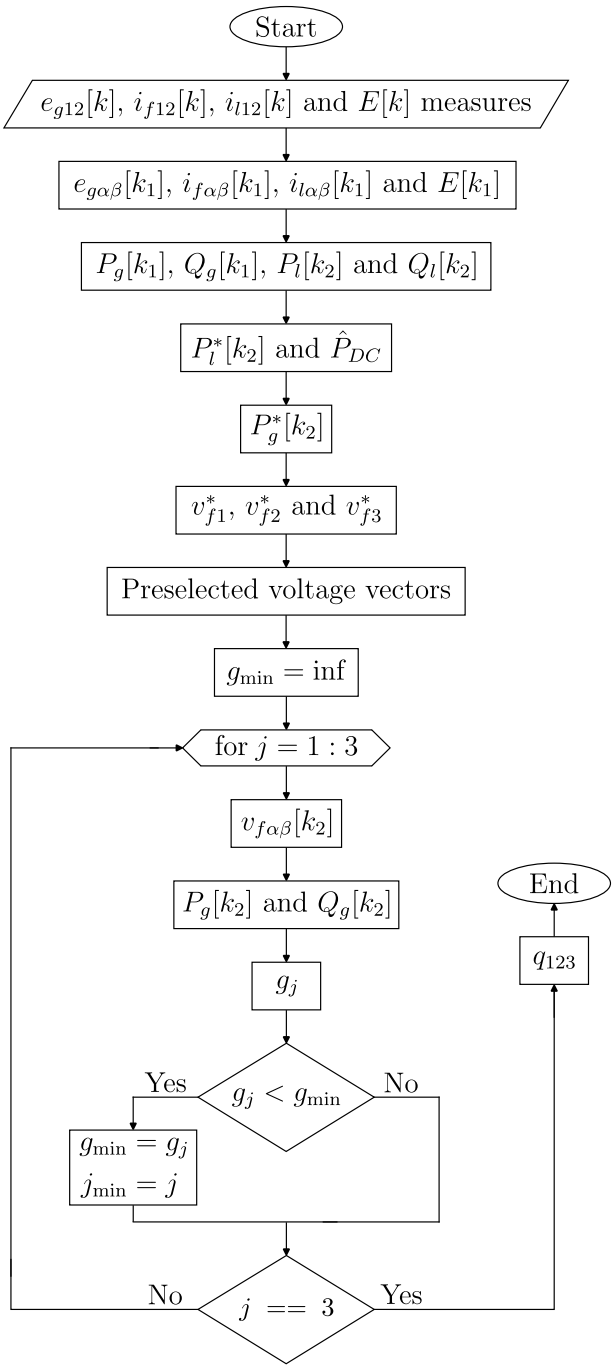

FIGURE 5. PPC flowchart.

for the SAPF is possible to identify the clamping region to reduce the amount of tests in the PPC.

Fig. 6 shows three regions that are obtained for three-phase balanced voltages. Therefore, using these regions it is possible to reduce the number of tests in the PPC. For instance, in the case of Region 1, where the reference voltage v_{f1}^* is the largest of all, leg 1 of SAPF is clamping at a high level, meaning that q_1 remains closed ($q_1 = 1$). Then, based on Table 1, the vectors V_4, V_5, V_6, and V_7 are chosen. Additionally, the regions can be divided into two

subregions, A and B, requiring only 3 tests in each subregion. For Subregion A, the vector possibilities are V_4, V_5, and V_7, while for Subregion B, the vectors are V_4, V_6, and V_7. Similarly, the highest voltages in regions 2 and 3 are v_{f2} and v_{f3}, respectively. This means that switches q_2 in Region 2 and q_3 in Region 3 will not change state and will remain high. Consequently, the number of tested vectors is reduced to 3, as summarized in Table 3.

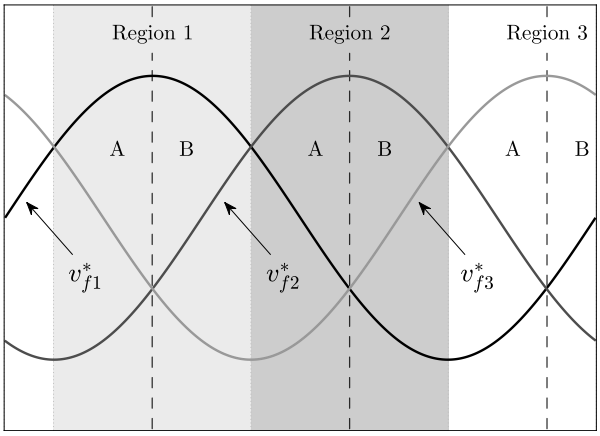

FIGURE 6. Clamping regions.

The active and reactive powers are used as a reference by the PPC. However, to optimize the vector selection of the SAPF, it is necessary to obtain the reference voltages using (5) and (6) and in the steady state, it is known that:

$$\frac{di_{f\alpha}}{dt} = -i_{f\beta} \tag{26}$$

$$\frac{di_{f\beta}}{dt} = i_{f\alpha} \tag{27}$$

then:

$$v^*_{f\alpha} = e_{g\alpha}[k_2] + r_f(i_{l\alpha}[k_2] - i^*_{g\alpha}) + l_f(i_{l\beta}[k_2] - i^*_{g\beta}) \tag{28}$$

$$v^*_{f\beta} = e_{g\beta}[k_2] + r_f(i_{l\beta}[k_2] - i^*_{g\beta}) + l_f(i_{l\alpha}[k_2] - i^*_{g\alpha}) \tag{29}$$

where the currents $i^*_{g\alpha}$ and $i^*_{g\beta}$ are obtained from the active and reactive reference power applied to the PPC, that is:

$$i^*_{g\alpha} = \frac{P^*_g e_{g\alpha}[k_2] + Q^*_g e_{g\beta}[k_2]}{e_{g\alpha}[k_2]^2 + e_{g\beta}[k_2]^2} \tag{30}$$

$$i^*_{g\beta} = -\frac{Q^*_g e_{g\alpha}[k_2] - P^*_g e_{g\beta}[k_2]}{e_{g\alpha}[k_2]^2 + e_{g\beta}[k_2]^2} \tag{31}$$

In addition, the reference voltages v^*_{f1}, v^*_{f2} and v^*_{f3} are obtained from $\alpha\beta$ voltages, i.e.:

$$v^*_{f1} = v^*_{f\alpha} \tag{32}$$

$$v^*_{f2} = -\frac{v^*_{f\alpha}}{2} + \frac{\sqrt{3}}{2} v^*_{f\beta} \tag{33}$$

$$v^*_{f3} = -\frac{v^*_{f\alpha}}{2} - \frac{\sqrt{3}}{2} v^*_{f\beta} \tag{34}$$

This analysis could be done for the opposite case to the regions presented in Fig. 6, that is, instead of considering the regions for when a reference voltage remains 120° greater than the others, consider the regions where the reference voltage remains 120° lower than the others, so instead of Region 1 being for when q_1 is at a high level, it would be for q_1 at a low level, $q_1 = 0$.

The SAPF leg can be clamped at a low level. When the voltage v_{f1} is at its minimum, the vectors are selected so that the switch q_1 remains open ($q_1 = 0$). Likewise, when v_{f2} is at its minimum, the switch q_2 is kept in the zero state ($q_2 = 0$); and when v_{f3} is at its minimum, the switch q_3 remains in the zero state ($q_3 = 0$).

TABLE 3. Preselected voltage vectors

Region		Subregion		Preselected voltage vectors
1	$v^*_{f1} > v^*_{f2}$ $v^*_{f1} > v^*_{f3}$	A	$v^*_{f3} > v^*_{f2}$	$V_4 - V_5 - V_7$
		B	$v^*_{f3} \leq v^*_{f2}$	$V_4 - V_6 - V_7$
2	$v^*_{f2} > v^*_{f1}$ $v^*_{f2} > v^*_{f3}$	A	$v^*_{f1} > v^*_{f3}$	$V_2 - V_6 - V_7$
		B	$v^*_{f1} \leq v^*_{f3}$	$V_2 - V_3 - V_7$
3	$v^*_{f3} > v^*_{f1}$ $v^*_{f3} > v^*_{f2}$	A	$v^*_{f2} > v^*_{f1}$	$V_1 - V_3 - V_7$
		B	$v^*_{f2} \leq v^*_{f1}$	$V_1 - V_5 - V_7$

V. SIMULATION RESULTS

The simulation results with the DPC and PPC (with optimized vector selection) control strategy applied to the SAPF are shown in this section. The studied system was simulated in PSIM® software. The same parameters are used for both strategies.

The parameters used to obtain the results are: voltage in the electrical grid equal to 127 V (RMS) and 60 Hz fundamental frequency, resistance and inductance for RL filter are, respectively, 0.5 Ω and 13 mH, resistance and inductance for RL load are, respectively, 0.3 Ω and 6 mH, DC-link reference voltage equal to 400 V, DC-link capacitance is equal to 2200 μF and the sampling period is equal to 50 μs. For the non-linear load, a full-bridge diode rectifier with a resistance of 50 Ω was used. The inductor filter design was realized using the conditions shown in Subsection B.

The gains proportional and integral of the PI controller for DC-link control are, respectively, $k_p = 0.2$ and $k_i = 3$. The parameter N used in (24) is equal to 100. Due to the similar behavior of switching between DPC and PPC strategies the same inductance can be used for both.

The waveforms of the grid voltage (e_{g1}) and the grid current (i_{g1}) are shown in Figs. 7(a) (for DPC) and 7(b) (for PPC). It is observed that, for both strategies, the current appears with a good sinusoidal shape and it is in phase with the grid voltage, that is, the power factor is unity, meaning that the correction of the power factor was performed properly. Figs. 7(c) (DPC) and 7(d) (PPC) show the grid currents, with approximately 6 A peak. Figs. 8(a) (DPC) and 8(b) (PPC) show the non-linear load currents with approximately the same peak current of the grid. Figs. 8(c) (DPC) and 8(d)

(PPC) show the SAPF currents, in which it is possible to see that there is harmonic components in the SAPF currents.

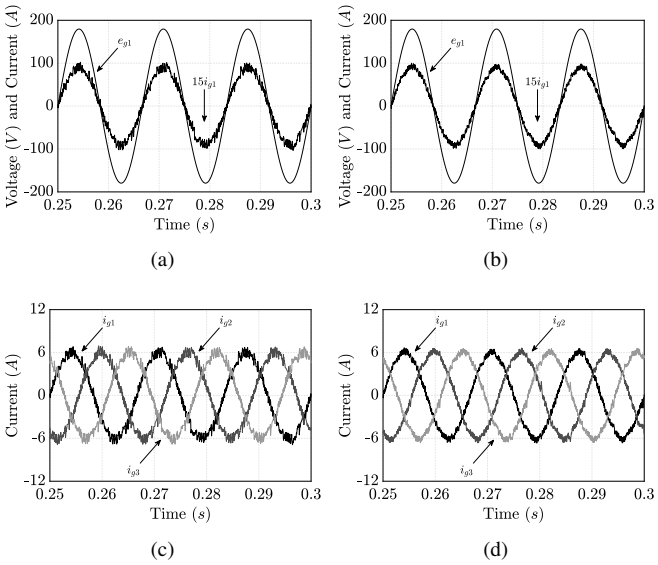

FIGURE 7. Simulation results. (a) Grid voltage and current for first phase, DPC. (b) Grid voltage and current for first phase, PPC. (c) Grid currents, DPC. (d) Grid currents, PPC.

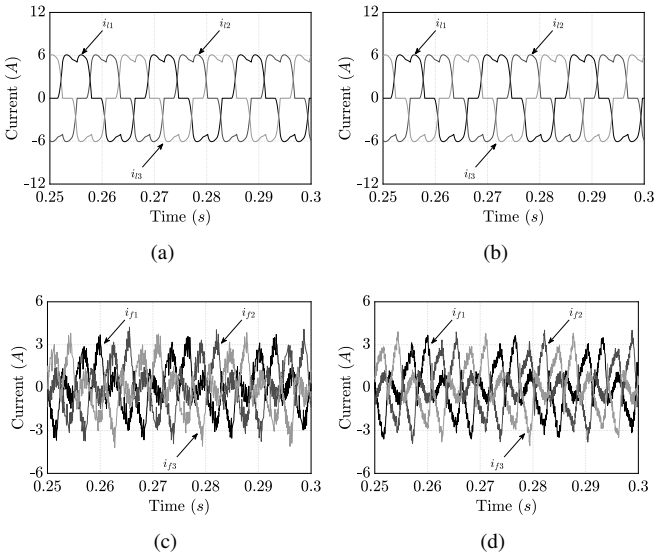

FIGURE 8. Simulation results. (a) Load currents, DPC. (b) Load currents, PPC. (c) SAPF currents, DPC. (d) SAPF currents, PPC.

Fig. 9(a) shows the SAPF voltage for the first phase using DPC strategy. Fig. 9(b) shows all voltage levels presented in Table 1. Figs. 9(c) (DPC) and 9(d) (PPC) show the control of the DC-link, in which it is possible to observe that the reference value E^* corresponds to the measured voltage.

Figs. 10(a) and 10(c) show, respectively, the active and reactive power for the SAPF using the DPC strategy, in which it is possible to observe that the reference values P_f^* and Q_f^* correspond to the measured powers and they

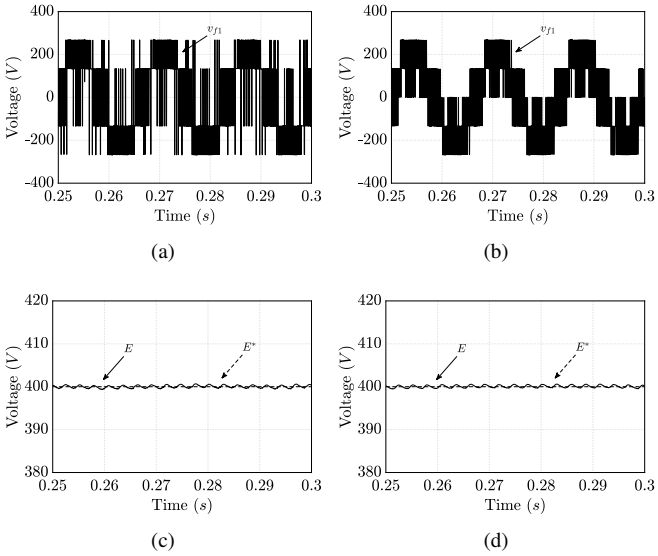

FIGURE 9. Simulation results. (a) SAPF voltage for first phase, DPC. (b) SAPF voltage for first phase, PPC. (c) DC-link voltage and reference, DPC. (d) DC-link voltage and reference, PPC.

are oscillating to compensate the harmonics in the grid, as also the instantaneous powers are correctly adjusted to reference values. Figs. 10(b) and 10(d) show, respectively, the active and reactive power in the electrical grid using the PPC strategy, in which it is possible to observe that the reference values P_g^* and Q_g^* correspond to the average measured powers, as also the instantaneous powers are correctly adjusted to reference values. To facilitate the visualization of the powers of SAPF and grid, an offset was intentionally inserted in Fig. 10.

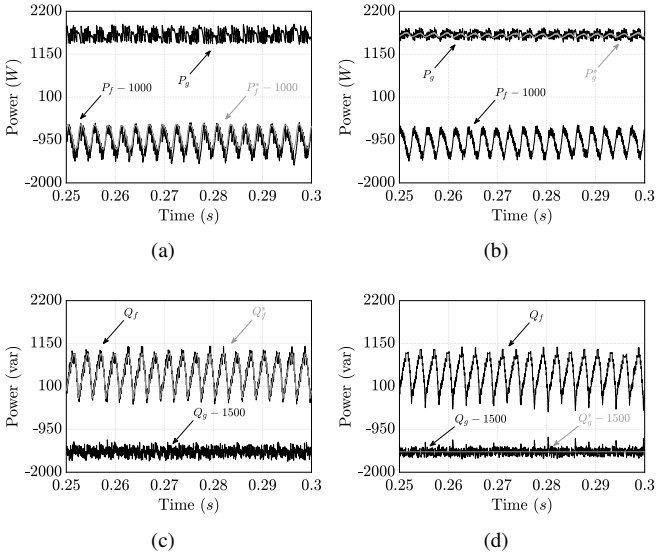

FIGURE 10. Simulation results. (a) Active power of grid, SAPF and reference P_f^*, DPC. (b) Active power of SAPF, grid and reference P_g^*, PPC. (c) Reactive power of grid, SAPF and reference Q_f^*, DPC. (d) Reactive power SAPF, grid and reference Q_g^*, PPC.

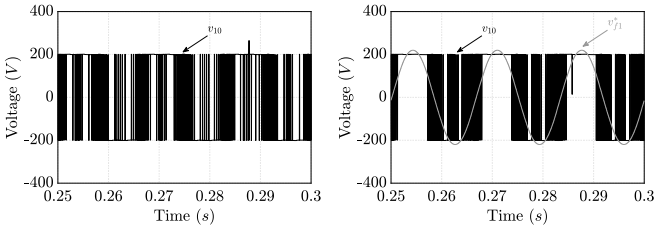

FIGURE 11. Simulation results. (a) v_{10} pole voltage, DPC. (b) v_{10} pole voltage and v_{f1}^* reference voltage, PPC.

Fig. 11 shows v_{10} pole voltage using DPC and PPC, so it can be seen that Fig. 11(a) is switching at high frequency and Fig. 11(b) during 120° is switching at low frequency. Furthermore, Fig. 11(b), the pole voltage v_{10} is fixed when v_{f1}^* is the highest reference voltage, i.e., switch q_1 is at high level, situation presented for Region 1 in Table 3.

Fig. 12 shows the behavior of the DC-link voltage and the grid current (i_{g1}) in a load transient from 75 Ω to 50 Ω, that is, an increase of 33% in charge. Therefore, it is noted that the two control strategies presented similar behavior, since both presented a small undershoot in the DC-link voltage and the current i_{g1} presented a smooth transition to the new current magnitude.

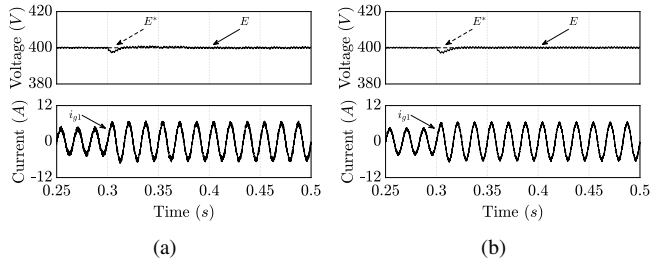

FIGURE 12. Simulation results for load transient. (a) DPC. (b) PPC.

VI. COMPARATIVE ANALYSIS

This section will present the comparison between strategies DPC and PPC. The parameters of analysis are: reduction of harmonic components, power semiconductor losses, root mean square error and average frequency switching. The analysis is based on results obtained from simulations.

TABLE 4. Total Harmonic Distortion for simulation results

	f_s	i_{g1}	i_{g2}	i_{g3}
DPC	20 kHz	8.77%	8.62%	8.62%
	32 kHz	5.70%	5.68%	5.68%
PPC	20 kHz	5.91%	6.08%	5.95%
PPC [12]	20 kHz	5.83%	5.70%	5.70%

Table 4 shows the Total Harmonic Distortion (THD) for strategies DPC and PPC. Two scenarios were considered: 1) sampling frequency equal to 20 kHz for both strategies and 2) approximately the same harmonic distortion for grid current, equal to 5,8%. For the same sampling frequency, the THD of PPC is smaller than that of DPC. The difference is close to 33%. On the other hand, for the same THD, the sampling frequency had to be increased to 32 kHz, which is an augmentation of 60% of sampling frequency, representing an increase in power loss.

Fig. 13 shows the reduction of harmonic components in the electrical grid for the strategies DPC and PPC, considering the sampling frequency is equal to 20 kHz. According to Fig. 13(a), the DPC strategy reduces the 5th and 7th harmonics of the grid current to 1.08% and 1.62%. Fig. 13(b) shows the harmonic components using PPC strategy, in which the SAPF reduced the 5th and 7th harmonics of the grid current to 1.6% and 1.15%. Therefore, both strategies were able to reduce the presence of 5th and 7th harmonics.

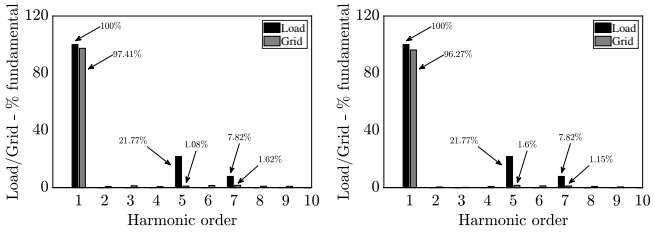

FIGURE 13. Simulation results for frequency spectra. (a) DPC. (b) PCC.

Table 5 shows the power semiconductor losses and average switching frequency ($\bar{f}_{sw}$) for both strategies. The power losses for each configuration were simulated using the IGBT-Module FS50R07N2E4 as a model, with the thermal module feature of the PSIM® software. The $\bar{f}_{sw}$ is obtained using the method presented in [21], that is:

$$\bar{f}_{sw} = \frac{n_1 + n_2 + n_3}{3T} \tag{35}$$

where n_1, n_2 and n_3 are the number of state changes of the switches for phases 1, 2 and 3 of the three-phase inverter and T is the period in which $\bar{f}_{sw}$ is evaluated. Thus, when comparing the PPC and DPC (for 20 and 32 kHz) note that for the conduction loss (P_{cd}) the results are similar. However, PPC provides smaller switching losses (P_{sw}) than DPC. Therefore, the PPC strategy presented lower total power losses (P_t) than DPC.

TABLE 5. Power semiconductor losses

	f_s	$\bar{f}_{sw}$	P_{cd}	P_{sw}	P_t
DPC	20 kHz	7060.32 Hz	2.89 W	7.51 W	10.40 W
	32 kHz	11146.39 Hz	2.83 W	10.95 W	13.79 W
PPC	20 kHz	6833.54 Hz	2.92 W	6.89 W	9.81 W
PPC [12]	20 kHz	6405.84 Hz	2.91 W	6.42 W	9.33 W

TABLE 6. Root Mean Square Error

	f_s	E	P	Q
DPC	20 kHz	0.31 V	193.39 W	106.72 var
	32 kHz	0.29 V	121.74 W	67.40 var
PPC	20 kHz	0.30 V	72.47 W	83.00 var
PPC [12]	20 kHz	0.32 V	72.54 W	84.70 var

Table 6 shows the Root Mean Square Error (RMSE) for both strategies. For DPC, the columns P and Q are related, respectively, with P_f and Q_f and for PPC they are related, respectively, with P_g and Q_g. Thus, it is possible to notice than for both strategies the DC-link RMSE is similar. For active power the PPC presented less RMSE than DPC (with the two f_s) . For reactive power, DPC presented lower RMSE than PPC for the sampling frequency of 32 kHz. Therefore, the PPC strategy demonstrates lower error than DPC.

Comparing the results of the present paper and [12], in Tables 4, 5 and 6, it is noted that there was no significant difference between PPC with or without vector selection optimization. This shows that the proposed PPC is able to provide virtually the same steady-state performance than PPC method discussed in [12], but with lower computational burden.

Using the `profiler` function of MATLAB®, it is possible to compare the processing time between the codes used in [12] and of this paper. The `profiler function` is a performance analysis that measures the processing time of code segments, providing detailed time information for each part of the code. Thus, comparing time values, it was noted that proposed PPC obtained a reduction in processing time of approximately 20% in relation to that discussed in [12].

VII. EXPERIMENTAL RESULTS

In order to validate the DPC and PPC strategies, experimental results were obtained in the laboratory. The experimental setup is based on a Digital Signal Processor (DSP) based on the Texas Instruments TMS320F28335 with a microcomputer equipped with appropriate plugin boards and sensors. The results were obtained by oscilloscope Agilent DSO-X 3014A 100 MHz. The sampling frequency is equal to 20 kHz, the DC-link voltage is equal to 400 V and the equivalent capacitance is equal to 1100 μF. The non-linear load is equal to that used in the simulations, but RL load was not used. The RL filter has the following parameters: resistance $r_f = 0.32\ \Omega$ and inductance $l_f = 9.5$ mH. The voltage in the three-phase grid is equal to 127 V (RMS) and 60 Hz fundamental frequency. The parameter N used in (24) is equal to 350. The other parameters were the same used in the simulation results.

Fig. 14 shows the experimental results for voltage and current in the electrical grid and DC-link voltage for DPC and PPC DC-link voltage equal to 400 V and a high power factor were obtained for both methods.. In addition, the grid voltage has harmonic components in high frequency but is more visible in DPC than in PPC. Fig. 15 shows the currents in the grid, in which it is possible to notice that the current in the grid is sinusoidal for both strategies. Figs. 16 and 17 show, respectively, the currents in the non-linear load and SAPF. In Fig. 18 it is possible to note that the grid current is sinusoidal because the SAPF compensates for the harmonic components of the load.

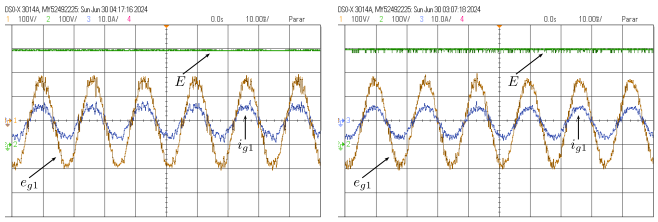

(a) (b)

FIGURE 14. Experimental results grid for first-phase voltage and current, and DC-link voltage. (a) DPC. (b) PCC.

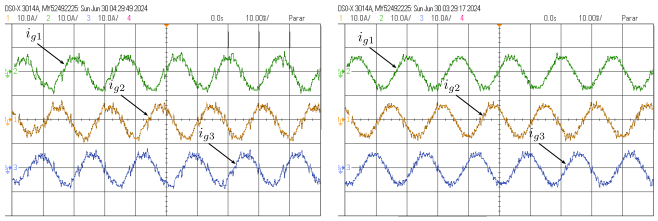

(a) (b)

FIGURE 15. Experimental results for grid currents. (a) DPC. (b) PCC.

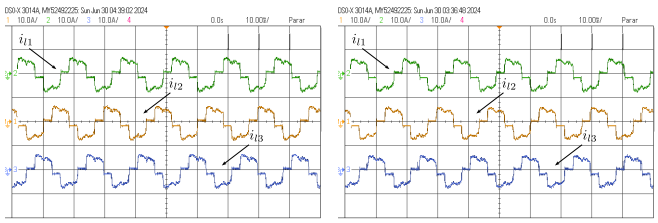

(a) (b)

FIGURE 16. Experimental results for load currents. (a) DPC. (b) PCC.

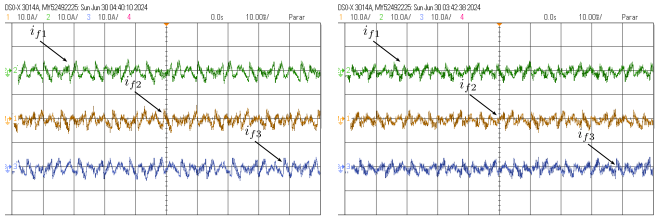

(a) (b)

FIGURE 17. Experimental results for SAPF currents. (a) DPC. (b) PCC.

Fig. 19 shows the behavior of the voltage on the DC-link and the current in the electrical grid (i_{g1}) in a load transient from 75 Ω to 50 Ω, that is, an increase of 33% charge. Different from the result obtained in the simulation, see Fig. 12, the DPC presented a better response during the load transient, since the system converged with less oscillation in both DC-link voltage and current in the electrical grid (i_{g1}), in addition to presenting lower undershoot for DC-link voltage. This behavior is due to a higher value of N, as N has an impact on the response time to obtain the new reference active power, that is, the higher N, the longer the time for the system to converge.

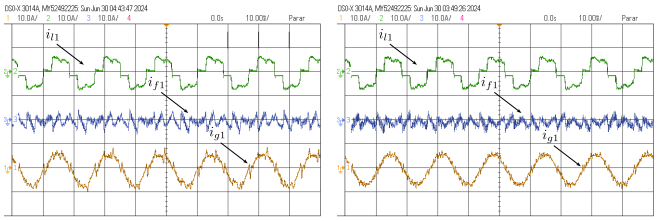

(a) (b)

FIGURE 18. Experimental results for first phase of the grid, load and SAPF currents. (a) DPC. (b) PCC.

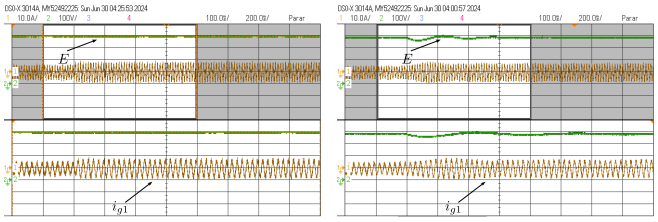

(a) (b)

FIGURE 19. Experimental results for load transient. (a) DPC. (b) PCC.

Table 7 shows the THD of the phase currents in the electrical grid. It is possible to see that PPC presented a better performance than DPC, with a difference of approximately 50% between them.

TABLE 7. Total Harmonic Distortion for experimental results

	f_s	i_{g1}	i_{g2}	i_{g3}
DPC	20 kHz	17.04%	15.32%	15.08%
PPC	20 kHz	6.30%	6.29%	5.96%

VIII. CONCLUSION

This article presented a comparison between two strategies for direct power control, in which one is based on hysteresis control and the other is based on FCS-MPC. Theses strategies are applied in a system composed of a three-phase electrical grid, one shunt active power filter and a non-linear load.

Based on the simulation results, both strategies provided grid currents with good sinusoidal shape, correction of power factor and proper regulation of DC-link voltage with a RMSE less than 0.35 V. Considering harmonic distortion, grid current THD obtained with PPC was lower than that of DPC. In addition, PPC presents lower switching frequency than DPC. At last, regulation of active and reactive power was performed by PPC, providing a lower RMSE value. Using optimization to select the optimal vector, it was possible to reduce processing time by approximately 20% compared to the strategy presented in [12].

Thus, the performance of the system using the PPC strategy was better than the DPC strategy, according to the simulation and experimental results presented in this article.

ACKNOWLEDGMENT

The authors would like to thank in part the Coordenação de Aperfeiçoamento de Pessoal de Nível Superior - Brasil (CAPES), Conselho Nacional de Desenvolvimento Científico e Tecnológico (CNPq) and grant 060/2023 Paraíba State Research Foundation (FAPESQ) for the financial support.

AUTHOR'S CONTRIBUTIONS

R. DA C. FERREIRA: Conceptualization, Data Curation, Formal Analysis, Investigation, Methodology, Resources, Software, Validation, Visualization, Writing – Original Draft, Writing – Review & Editing. P. H. M. MARTINS: Conceptualization, Data Curation, Formal Analysis, Investigation, Methodology, Resources, Software, Validation, Visualization, Writing – Original Draft, Writing – Review & Editing. N. ROCHA: Conceptualization, Data Curation, Formal Analysis, Funding Acquisition, Investigation, Methodology, Project Administration, Resources, Software, Supervision, Validation, Visualization, Writing – Original Draft, Writing – Review & Editing. E. R. C. SILVA: Conceptualization, Formal Analysis, Methodology, Writing – Original Draft, Writing – Review & Editing. V. F. M. B. MELO: Conceptualization, Formal Analysis, Investigation, Methodology, Resources, Writing – Original Draft, Writing – Review & Editing.

PLAGIARISM POLICY

This article was submitted to the similarity system provided by Crossref and powered by iThenticate – Similarity Check.

REFERENCES

[1] S. Hao, Z. Fu, Q. Wang, J. Zheng, M. Zhang, "A Novel Control Strategy for Shunt Active Power Filter under Nonlinear and Unbalanced Three Phase Load Conditions", *in 2016 International Symposium on Computer, Consumer and Control (IS3C)*, pp. 96–98, 2016, doi:10.1109/IS3C.2016.35.

[2] S. S. Patil, R. A. Metri, O. K. Shinde, "Shunt active power filter for MV 12-pulse rectifier using PI with SMC controller", *in 2017 International Conference on Circuit ,Power and Computing Technologies (ICCPCT)*, pp. 1–6, 2017, doi:10.1109/ICCPCT.2017.8074260.

[3] J. Afonso, C. Couto, J. Martins, "Active Filters with Control Based on the p-q Theory", *IEEE Industrial Electronics Society Newsletter*, vol. 47, 01 2000.

[4] H. Afghoul, F. Krim, "Comparison between PI and fuzzy DPC control of a shunt active power filter", *in 2012 IEEE International Energy Conference and Exhibition (ENERGYCON)*, pp. 146–151, 2012, doi:10.1109/EnergyCon.2012.6347742.

[5] F. Ronchi, A. Tilli, "Design methodology for shunt active filters", *Proc 10th EPE-PEMC 2002*, 01 2002.

[6] A. Chaoui, J.-P. Gaubert, A. Bouafia, "Direct power control concept and analysis for three phase shunt active power filter", *in IECON 2012 - 38th Annual Conference on IEEE Industrial Electronics Society*, pp. 1286–1294, 2012, doi:10.1109/IECON.2012.6388553.

[7] H. A. Young, M. A. Perez, J. Rodriguez, H. Abu-Rub, "Assessing finite-control-set model predictive control: A comparison with a linear current controller in two-level voltage source inverters", *IEEE Industrial Electronics Magazine*, vol. 8, no. 1, pp. 44–52, 2014.

[8] S. Vazquez, J. I. Leon, L. G. Franquelo, J. Rodriguez, H. A. Young, A. Marquez, P. Zanchetta, "Model Predictive Control: A Review of Its Applications in Power Electronics", *IEEE Industrial Electronics Magazine*, vol. 8, no. 1, pp. 16–31, 2014, doi:10.1109/MIE.2013.2290138.

[9] C. Castillo, C. Garcia, P. Acuna, "Hierarchical Line-to-Line Voltage-Based FCS-MPC Computational Cost Reduction for Multi-Level Converters", *in 2023 IEEE 8th Southern Power Electronics Conference and 17th Brazilian Power Electronics Conference (SPEC/COBEP)*, pp. 1–7, 2023, doi:10.1109/SPEC56436.2023.10408524.

[10] T. Martins Bezerra, N. Rocha, A. De Medeiros Maciel, E. Luiz Lopes Fabrício, K. Bezerra De Carvalho, "Predictive Control Applied to Three-Phase Four-Wire Shunt Active Power Filters: An Innovative Approach", *in 2023 IEEE 8th Southern Power Electronics Conference and 17th Brazilian Power Electronics Conference (SPEC/COBEP)*, pp. 1–7, 2023, doi:10.1109/SPEC56436.2023.10408551.

[11] R. da Cruz Ferreira, S. M. A. Dias, N. Rocha, E. R. C. da Silva, V. F. B. Melo, "Predictive Control for a Single-Phase to Three-Phase Converter with Two-Parallel Single-Phase Rectifiers", *Eletrônica de Potência*, vol. 28, no. 4, pp. 324–336, 2023.

[12] R. da Cruz Ferreira, P. H. De Morais Martins, N. Rocha, E. R. C. Da Silva, V. F. M. B. Melo, "Comparison Between Conventional and Model Predictive Control for Direct Power Control Applied to a Shunt Active Power Filter", *in 2023 IEEE 8th Southern Power Electronics Conference and 17th Brazilian Power Electronics Conference (SPEC/-COBEP)*, pp. 1–8, 2023, doi:10.1109/SPEC56436.2023.10408635.

[13] J. P. Silva, J. R. P. De Assis, D. A. Fernandes, N. Rocha, A. J. S. Filho, "Performance of Predictive Control Applied to Active Power Filter", *in 2023 IEEE Applied Power Electronics Conference and Exposition (APEC)*, pp. 2888–2894, 2023, doi:10.1109/APEC43580.2023.10131190.

[14] O. Kukrer, "Discrete-time current control of voltage-fed three-phase PWM inverters", *IEEE Transactions on Power Electronics*, vol. 11, no. 2, pp. 260–269, 1996, doi:10.1109/63.486174.

[15] D. Daftary, M. T. Shah, "Design and Analysis of Hybrid Active Power Filter for Current Harmonics Mitigation", *in 2019 IEEE 16th India Council International Conference (INDICON)*, pp. 1–4, 2019, doi:10.1109/INDICON47234.2019.9029052.

[16] A. V. Barva, P. R. Bhavsar, "Design and simulation of four-leg based three-phase four-wire shunt active power filter", *in 2018 International Conference on Communication information and Computing Technology (ICCICT)*, pp. 1–6, 2018, doi:10.1109/ICCICT.2018.8325868.

[17] B. S. Chen, G. Joos, "Direct Power Control of Active Filters With Averaged Switching Frequency Regulation", *IEEE Transactions on Power Electronics*, vol. 23, no. 6, pp. 2729–2737, 2008, doi:10.1109/TPEL.2008.2004958.

[18] V. Kaura, V. Blasko, "Operation of a phase locked loop system under distorted utility conditions", *IEEE Transactions on Industry Applications*, vol. 33, no. 1, pp. 58–63, 1997, doi:10.1109/28.567077.

[19] L. Tarisciotti, A. Formentini, A. Gaeta, M. Degano, P. Zanchetta, R. Rabbeni, M. Pucci, "Model Predictive Control for Shunt Active Filters With Fixed Switching Frequency", *IEEE Transactions on Industry Applications*, vol. 53, no. 1, pp. 296–304, 2017, doi:10.1109/TIA.2016.2606364.

[20] M. H. Nguyen, S. Kwak, S. Choi, "Model Predictive Based Direct Power Control Method Using Switching State Preference for Independent Phase Loss Decrease of Three-Phase Pulsewidth Modulation (PWM) Rectifiers", *IEEE Access*, vol. 12, pp. 5864–5881, 2024, doi:10.1109/ACCESS.2024.3350191.

[21] V. Yaramasu, B. Wu, *Model predictive control of wind energy conversion systems*, John Wiley & Sons, 2016.

BIOGRAPHIES

Ruben da Cruz Ferreira born in João Pessoa, Paraíba, Brazil, in 2000. He is a bachelor's student in electrical engineering from the Federal University of Paraíba, João Pessoa, Brazil. Since 2019, he is working in researches about shunt active power filters and power converters. His research interests include power electronics, renewable energy sources and electrical drives.

Pedro Henrique de Morais Martins is a master's student in the Postgraduate Program in Renewable Energy (PPGER) at UFPB. Bachelor of Electrical Engineering from the Federal University of Paraíba (UFPB). Former scholarship holder of the BRAFITEC program, funded by the Coordination for the Improvement of Higher Education Personnel - CAPES, where he spent one year of sandwich undergraduate studies at IMT-Atlantique in Nantes, France. He was part of the UFPB PET-Electric Group from April 2018 to September 2020. He holds a technical degree in Accounting from the Federal Institute of Education, Science and Technology of Paraíba (IFPB). His interests are focused on Energy Systems and Power Electronics, including Industrial Electronics, Power Electronics, generation, transmission, and distribution of electric power, protection of electrical systems, electrical machines, electrical drives and controls, and renewable energy sources.

Nady Rocha born in São Gabriel, Bahia, Brazil, in 1982. He received the B.S., M.S. and Ph.D. degrees in electrical engineering from the Federal University of Campina Grande, Brazil, in 2006, 2008 and 2010, respectively. Since 2011, he has been with the Department of Electrical Engineering, Federal University of Paraíba, João Pessoa, where he is currently an Associate Professor of Electrical Engineering. His research interests include power electronics, renewable energy sources, and electrical drives.

Edison Roberto Cabral da Silva received the B.S.E.E. degree from the Polytechnic School of Pernambuco, Recife, Brazil, in 1965, the M.S.E.E. degree from the University of Rio de Janeiro, Brazil, in 1968, and the Dr. Eng. degree from the University Paul Sabatier, Toulouse, France, in 1972. He was the Director of the Research Laboratory on Industrial Electronics and Machine Drives, LEIAM, Campina Grande, Brazil, for 30 years. He is currently Professor Emeritus at both University of Campina Grande, UFCG, and University of Paraiba, UFPB, where he is still acting. His current research work is in the area of power electronics and renewable energy systems. Co-author of the book entitled "Advanced Power Electronics Converters: PWM Converters Processing AC Voltages", IEEE/Wiley, he is a member of the Brazilian Society on Power Electronics, SOBRAEP (Honorable), Brazilian Society on Automatic Control, SBA, and IEEE (Life-Fellow). He is also a SBA Past-President.

Victor F. M. Bezerra Melo born in Pesqueira, Brazil, in 1988. He received the B.S., M.S., and Ph.D. degrees in electrical engineering from the Federal University of Campina Grande, Campina Grande, Brazil, in 2012, 2013, and 2017, respectively. From October 2014 to June 2018 he was with Federal Institute of Technology of Pernambuco (IFPE), Afogados da Ingazeira, Brazil, where he was a Professor. Since June 2018 he has been with the Renewable Energies Department, Federal University of Paraíba, where he is currently a Professor. His current research interests include power electronics, static converters, and electrical drives.